The International Journal of Advanced Manufacturing Technology (2019) 100:1787–1799
https://doi.org/10.1007/s00170-018-2717-z

ORIGINAL ARTICLE

Effect of ultrasonic vibration on welding load, macrostructure, and mechanical properties of Al/Mg alloy joints fabricated by friction stir lap welding

S. Kumar[1] · C. S. Wu[1] · S. Zhen[1] · W. Ding[1]

Received: 20 June 2018 / Accepted: 17 September 2018 / Published online: 9 October 2018

Abstract
An initial study is proposed in order to evaluate the outcomes of ultrasonic vibration in friction stir welding of Al and Mg alloys for lap configuration. A novel ultrasonic assembly is designed and developed such that ultrasonic vibrations could be enforced along the welding direction into the weldment via the welding tool. Various sets of welding parameters are picked out for experimentation and thereafter optimum are evaluated. With ultrasonic assistance during pin and shoulder plunging, a substantial diminution in welding load, up to 30 and 19.75% are obtained while the noteworthy reduction in tool torque and input power is also perceived at optimum parameters. Additionally, lap shear tests result into an improvement of 37.88 and 39.24%, respectively, in context to failure load and weldment elongation. Macrostructure analysis portrays elimination of defects, enhanced material mixing, and broadening of the stirred zone with acoustic assistance.

Keywords Friction stir lap welding · Ultrasonic vibration · Macrostructure · Mechanical properties · Aluminum alloy · Magnesium alloy

1 Introduction

Mg alloys are the lightest metals found on the earth and one of the third most commonly used structural metals after iron and aluminum. Nowadays, they are being integrated into numerous structural parts in countless applications in order to obtain substantial weight reduction [1]. Integration of Al and Mg alloys together could significantly enhance structural flexibility and reduce structural weights as well as improve mechanical properties. However, it is difficult to obtain sound welding of both the metals together due to poor weldability, a large gap in melting point temperature, and the brittle nature of Mg alloys. Various conventional welding methods such as vacuum diffusion bonding [2, 3], laser welding [4], and gas metal arc plug welding [5] have been attempted in the past. However, none of them is universally consented due to various shortcomings such as defect formation, poor weld quality, loss of mechanical strength, and formation of an intermetallic compound layer [1, 6].

In the last few decades, the friction stir welding (FSW) technique has gotten a wide acceptance to join various grades of similar and dissimilar Al alloys [7–14]. Besides, it has also been proven quite efficacious to join various grades of Al and Mg alloys with adequate weld strength [15–20]. In conventional friction stir lap welding (CFSLW) of Al/Mg alloys, a considerable amount of constitutional liquation occurs into the weldment due to the heat and welding load (axial force) which enhances the formation of intermetallic compound (IMCs) layers of nature $Al_{12}Mg_{17}$ and Al_3Mg_2 [21–23]. These IMCs are brittle and structurally fragile, and substantially degrade the weldment strength [22, 24]. A lower rotation and higher welding speed may introduce a lesser heat input but might suffer from poor bonding. Mohammadi et al. pointed out that welding speed was a primary factor to obtain sound FSW joints of Al/Mg alloys, as it might significantly alter weldment properties [18]. They reported cleavage cracks and protuberances to characterize the brittle fracture mode, depicting

✉ C. S. Wu
wucs@sdu.edu.cn

[1] MOE Key Lab for Liquid-Solid Structure Evolution and Materials Processing, Institute of Materials Joining, Shandong University, Jinan 250061, China

cracks and failure were developed from the intermetallic in the Al/Mg abutting layer [25]. At a higher rotation speed, the weld bond depth was decreased due to inadequate material mixing. It resulted in the degraded strength of a dissimilar lap joint [26]. Tan et al. [27] narrated that either too low or too high heat input facilitated defect formation and should be optimized. Firouzdor et al. [28] observed crack formation at the joint center during CFSLW, when the Al alloy was placed at the top. Chen et al. [22] obtained enhanced weld strength at a lower welding speed when Al alloy was placed at the top. Ji et al. studied about the pin adhesion problem during the FSW of Al and Mg alloys. They concluded that the adhesion phenomenon was due to higher heat input into the weld nugget zone (WNZ) which deteriorated joint properties [29]. Some of the notable literature in context to Al/Mg alloy CFSLW is presented in Table 1.

During CFSLW, the presence of IMCs at the Al-Mg alloy weld interface is still observed which is responsible for substantial loss of weld strength [30]. Therefore, it is vital to control IMC layer formation to achieve sound Al/Mg welds.

As ultrasonic vibrations have a long-lasting history of metal processing and joining to cope with various conventional shortcomings [31–34], they have also been implemented successfully in conjunction with CFSLW to weld various grades of Al alloys both for butt and lap configuration [35–40]. During ultrasonic assistance, ultrasonic vibrations are directly and dynamically transported into the localized region of the weldment. It leads to acoustic softening with the plastic deformation in the shear layer of the weldment. It is worth noting that reported studies on ultrasonic assistance in Al/Mg alloy FSW are too scarce [41–44]. Ji et al. applied ultrasonic assistance along the FSW tool during welding of Al/Mg alloys. They showed improved material mixing and increased mechanical interlocking between the two metals [41]. Benfer et al. applied ultrasonic assistance at a distance from the weldment and concluded there were improved tensile strength and suppression of the IMC layers [42]. Strass et al. applied ultrasonic vibrations by passing them through the backing plate [44] and concluded there was an increment of 30% Al/Mg alloy weldment strength. It is interesting to note that quite a few ultrasonic assembly designs are reported in past literature addressing the integration of ultrasonic vibrations into the FSW process [37, 42, 44–46]; however, most of them apparently either lack the adequate and efficient transfer of ultrasonic energy into the weldment [42, 44] or suffered from frequent failures of horn attachments [37]. All these shortcomings result into a marginal or no effect of ultrasonic vibration on welding load diminution and improvement in weldment strength. As ultrasonic vibrations possess the tendency to be absorbed in a localized region, they can be more effective if applied directly into the WNZ via rigid contacts. In order to cope with the aforesaid deficiencies, authors have designed and developed a new ultrasonic system that could efficiently

Table 1 Important outlines of past literature reported on FSLW of Al-Mg

Workpiece material and position	Thickness (mm)/joint type	Process parameters	Tool parameters	Key findings	References
AA6022-T4/Mg alloy AM60B, Al(T), Mg(B)	1.5 and 3.1	RS: 1500–4500 WS: 20–90	TM: H13 TS, SD: 12, PD: 5.4, PL: 2.4, PP: triangular, SP: concave, TTA: 3^0, OL: 30, PE: 0.2	OP: 1500 rpm and 50 mm/min, LSS: 3.3 kN at 1500 rpm, IMC: $Al_{12}Mg_{17}$ and Al_3Mg_2, HD: 102 HV	[28]
6061 Al/AZ31B Mg, T-B and B-T	1.6	RS: 800 and 1400 WS: 38	TM: H13 TS, SD: 10, PD: 4, PL: 1.5, 2.3 (Lap), PP: threaded, SP: concave, TTA: 3^0, OL: 38	IMCs: $Al_{12}Mg_{17}$ and Al_3Mg_2 HI: Mg(B)-Al(T) > Mg(T)-Al(B)	[14]
AZ31B-H24 Mg/AA5754-O Al alloy, T-B and B-T	2.0	RS: 2000 (FSSW)	TM: H13 TS, SD: 13, PD: 5, PL: 2.8, PP: threaded, SP: scrolled, TTA: NR, PE: 0.2	IMCs: $Al_{12}Mg_{17}$ and Al_3Mg_2 HD: 125 HV FL: Mg/Al adhesive> Al/Mg adhesive	[15]
Al 6061 alloy/AZ31B Mg alloy, AZ31B (T), Al 6061 (B)	2.3 and 3.1	RS: 560, 700, 900, 1250, 1400 WS: 16, 20, 25, 31, 40	TM: H13 TS, SD: 18, PD: 5–6, PL: 4.5, PP: tapered threaded, SP: concave, TTA: 3^0	IMCs: $Al_{12}Mg_{17}$ and Al_3Mg_2, OP: 1400 RPM and 40 mm/min, LSS: 6.5 kN, HD: 302 HV (max)	[16]
Al 6061 alloy/AZ31B Mg alloy, AZ31B (T), Al 6061 (B)	2.3 and 3.1	RS: 560–1400 WS: 16–40	TM: H13 TS, SD: 18, PD: 5–6, PL: 4.5, PP: tapered threaded and tapered, SP: concave, TTA: 3^0	IMCs: $Al_{12}Mg_{17}$ and Al_3Mg_2, LSS: 6492 N (max) at 1400 rpm and 40 mm/min, HD: 325 HV (max)	[22]

B bottom position in lap welding, *T* top position in lap welding, *RS* rotation speed in RPM, *WS* welding speed in mm/min, *TM* tool material, *SD* shoulder diameter in mm, *PD* pin diameter in mm, *PL* pin length in mm, *PP* pin profile, *SP* shoulder profile, *TTA* tool tilt angle, *IMCs* intermetallic compounds, *HI* heat input, *NR* not reported, *HD* hardness, *OP* optimum parameters, *LSS* lap shear strength, *FL* fatigue life

transfer ultrasonic energy along the welding direction into the weldment via the FSW tool [47]. The contact points in such an ultrasonic assembly are kept rigid so as to ensure the safe and efficient transfer of acoustic energy over the weldment surface. In order to evaluate the efficacy of such an ultrasonic system over the CFSLW process, a series of comparative experimentation is made in context to measuring the welding load, torque, and power as well as mechanical and macrostructural properties of Al/Mg alloy weldment for a wide range of welding parameters.

2 Experimental procedure

2.1 Ultrasonic vibration assembly

A novel ultrasonic vibration setup is designed, developed, and integrated into the conventional milling machine such that the ultrasonic vibrations can be applied along the welding direction into the weldment via the FSW tool. The ultrasonic setup comprises a horn, transducer, and generator where the ultrasonic horn and transducer are rigidly fixed into the machine structure using in-house developed fixtures. Ultrasonic vibration assembly is meant to operate under the efficient power of 3000 W to yield 20 kHz frequency and 25 μm amplitude during ultrasonic vibration assisted friction stir lap welding (UVaFSLW). A detailed study of the ultrasonic assembly used in this work can be quoted from the authors' previous work [47]. Requisite adjustments are attained to utilize a 2.0 T HONGHAI-made conventional milling machine to work under the CFSLW framework. The machine is equipped with a servo control system to drive the worktable along the x and y directions. Vertical motion (along the z direction) of the tool is controlled by a hydraulic cylinder. The position of the x, y, and z axes can be defined using a remote-controlled system and can also be set via NC programming. A sensor system is attached to the milling machine for measuring real-time variation in welding load (axial force F_z) and tool torque during the pin/shoulder plunging and tool travel. Figure 1 shows a schematic of the ultrasonic vibration system integrated into a conventional milling machine. During UVaFSLW, ultrasonic vibrations are transmitted to the lapped surfaces of Al/Mg alloys through a specially designed FSW tool as well as via the front part mounted at the horn face.

2.2 Materials and methods

6061 aluminum alloy and AZ31B Mg alloy plates of 3.0 mm thickness are used to fabricate dissimilar metal CFSLW and UVaFSLW joints. Plates of dimension 300 × 80 mm^2 are cut from bulk sheet volume using a band saw such that the maximum dimension coincides with the rolling direction. The top, bottom, and lapped surfaces of both of the metal plates are

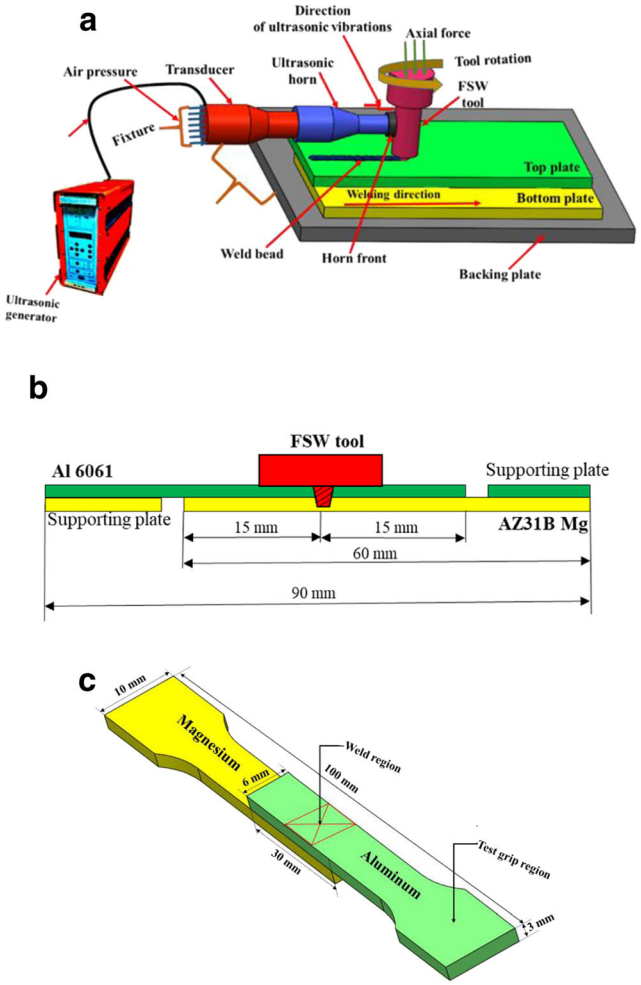

Fig. 1 **a** Schematic of ultrasonic vibration integration and a typical FSLW process. **b** Dimensional sketch of Al and Mg plates. **c** Details of the lap shear test sample

polished and subsequently cleaned with acetone before welding. Table 2 lists the nominal chemical composition of AZ31B Mg alloy and 6061 Al alloy. A specially designed FSW tool is employed for CFSLW and UVaFSLW of Al/Mg and has a shoulder diameter 20.0 mm with a threaded pin of length 5.6 mm. The maximum and minimum diameters of the threaded pin are 6.0 and 3.0 mm, respectively, and the tool material is H13 tool steel. The FSW tool is quenched and subsequently tempered to achieve a hardness of 60 HRC to improve its wear resistance. Experiments are performed with a tilt angle of 3° with respect to the tool vertical axis, and the plunge depth is kept constant in all experiments, equal to 0.1 mm. The overlap length of each plate is kept up to 30 mm for CFSLW and UVaFSLW. Various sets of welding parameters are chosen to determine optimum parameters by placing Al and Mg at the top and bottom, respectively. However, outcomes of 600–1200 rpm rotational speed and 50–250 mm/min welding speed are presented for analysis in the present work. For the sake of simplicity, the welding parameters are denoted as 600/50, 800/100, and so on, where

Table 2 The chemical composition of AZ31B Mg and 6061 Al alloys

Alloy	Al	Zn	Mg	Mn	Si	Cu	Cr	Fe	Ti	Ca
AZ31B Mg alloy	2.5–3.5	0.25 max	Balance	0.2–0.1	0.1 max	0.05 max	–	0.7 max	0.15 max	–
6061 Al alloy	Balance	0.1 max	0.8–1.2	0.15 max	0.4–0.8	0.15–0.4	0.04–0.35	–	–	0.04 max

600 and 800 rpm represent the rotational speeds and 50 and 100 mm/min are the welding speeds.

2.3 Metallographic examination

CFSLW and UVaFSLW Al/Mg weld samples are sectioned perpendicular to the weld direction, i.e., in the plane of the weld cross sections. The samples are grounded and polished using different sets of emery papers up to 1200 grit followed by 1 mm diamond slurry and 0.04 mm colloidal silica. Both Al and Mg weld parts are etched with the solution of 20 g NaOH in 100 ml deionized water for 55 s and Nital (0.5% HNO_3 ethanol solution) for 15 s to reveal Al and Mg macrostructures, respectively. Al is colored using a solution of 5 g $KMnO_4$ and 1 g NaOH in 100 ml distilled water for 12 s. The macrostructure is examined using a ZEISS-made Daheng Invasion USB camera microscope.

2.4 Mechanical testing

CFSLW and UVaFSLW Al/Mg weld samples are cut as per ASTM standard transverse to the welding direction using a wire cut electro-discharge machine as shown in Fig. 1c. A SANS YYL-20 universal testing machine operated in displacement control mode is used to perform tensile testing at room temperature (22 °C) with a constant crosshead speed of 1 mm/min. At least three repetitions for each condition are performed under identical conditions, and the surface of the specimen is polished with grade 240 abrasive papers. For microhardness measurements, both the samples (CFSLW and UVaFSLW) are sectioned perpendicular to the welding direction and subsequently cold mounted using non-conducting epoxy powders. Furthermore, they are polished with a set of emery papers of different grades. Final polishing is done with diamond paste using a variable-speed grinder polishing machine (Buehler, Ecomet 3000). A Vickers hardness indentation machine (UHL VMHT 001) with 200 gmf with 15 s dwell time is used to obtain the microhardness profile of the welded sample in a cross section normal to the welding direction.

3 Results and discussion

3.1 Welding load, torque, and power variation in CFSLW and UVaFSLW of Al/Mg alloys

A comparative analysis of welding load, torque, and power during CFSLW and UVaFSLW is performed. Various sets of parameters ranging from 600 rpm to 1200 rotational speed and 50 to 250 mm/min welding speed are used to determine the optimum parameters. It is evident that welds made with 800 rpm rotational speed and 100–150 mm/min welding speed show good results. Subsequent analysis of the welding load, torque, and power at different sets of parameters is presented and discussed in the following sections.

3.1.1 Welding load analysis

A variation in welding load for Al/Mg alloys CFSLW and UVaFSLW (Al at the top) under parameters 800/100 and 800/150 is depicted in Fig. 2. Results depict that ultrasonic vibrations pose a substantial diminution in welding load during the pin, shoulder plunging, and minor effects during tool

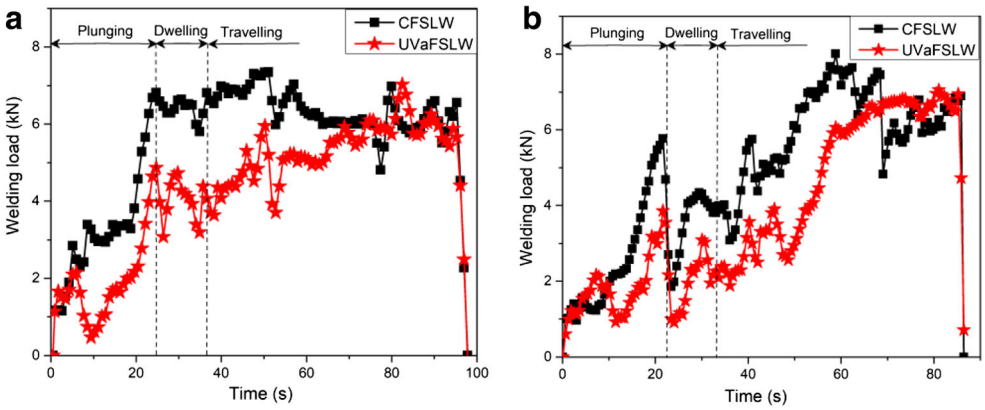

Fig. 2 Welding load comparison for CFSLW and UVaFSLW at **a** 800 rpm and 100 mm/min and **b** 800 rpm and 150 mm/min

traveling. For UVaFSLW at 800/100, an equivalent welding load diminution, up to 29.32 and 22.12%, is foreseen during pin and shoulder plunging, respectively (Fig. 2a). In case of tool traveling, ultrasonics apparently do not pose any notable effect on welding load diminution. A similar pattern of notable reduction in welding load up to 30.01 and 19.75% during pin and shoulder plunging, respectively, is also evident for 800/150. An equivalence drift in welding load reduction but quite lesser in magnitude has been documented by Kumar [37] and Park et al. [46] during ultrasonic-assisted FSW of Al alloys in butt configuration. In our newly designed ultrasonic setup, required modifications are made to ensure an efficient and rigid contact of the horn end face with the FSW tool. It facilitates and ensures the efficient transfer of acoustic energy at the area of interest. A reduction in welding load can be attributed to the fact that when ultrasonic vibrations are imparted into the weldment vicinity, they enhance the material mixing [41] and also lead to additional softening of the workpiece material [48], which in turn reduces the material flow stress [45]. Frequent contact of the FSW tool with the metal cold part yields frictional resistance and thus increases the temperature of the material just below it. It makes the material softer and allows easy penetration of the tool pin and shoulder. It can also be noted that variation in welding load is quite uniform for CFSLW compared to UVaFSLW (Fig. 2). It is because, when high-frequency ultrasonic vibrations are directed into the weldment via the FSW tool, the bottom part of the tool (pin) follows a to-and-fro motion at the micron level. It makes periodic contacts of the tool pin with that of the workpiece surface, and hence has multiple peaks in the welding load graph.

Investigation of the welding load profile (peak-to-peak comparison for a given parameter) during CFSLW and UVaFSLW of Al/Mg alloys at different welding (50–250 mm/min and constant rotation speed) and rotation (600–1200 rpm and constant welding speed) speeds is presented in Fig. 3.

When the rotation speed is kept constant (equal to 600 rpm) and the welding speed is varied from 50 to 250 mm/min, notable welding load diminution takes place at 600/150 and 600/100, equal to 9.5 and 7.2%, respectively, while on other parameters such as 600/50, 600/200, and 600/250, ultrasonic vibration apparently does not have any notable effects (Fig. 3a). In the same way, at a constant rotation speed of 800, a significant welding load reduction is reported at 800/150 and 800/100, equal to 14.22 and 8.2%, respectively. Ultrasonic vibrations seem to have negative effects on welding load reduction under parameters 800/50 and 800/200 (Fig. 3a). For constant rotation speeds of 1000 and 1200 rpm, the maximum reduction in welding load occurs at 1000/100 and 1200/150, equal to 9.3 and 7.3%, while its minima lie at 1000/250 and 1200/50.

When the welding speed is kept constant (50 and 100 mm/min) and the rotation speed is varied from 600, 800, 1000, and 1200 rpm, maximum reduction in welding load (comparing maximum values for a given parameter) comes out at 1000/50 and 1000/100 equal to 6.25 and 9.5%, while ultrasonic vibrations seem to have a negative effect at 1200/50 and 800/50 (Fig. 3b). In the case of 100 mm/min constant welding speed, ultrasonic vibration seems to have a positive influence on all welding parameters equal to 7.2, 8.10, 9.5, and 1.95% at 600/100, 800/100, 1000/100, and 1200/100, respectively. For a constant welding speed (150, 200, and 250 mm/min), the maximum drop in welding load occurs at 800/150, 800/200, and 1200/250 equal to 14.11, 5.95, and 2.11%, respectively. While on other parameters except 1000/150 (7.84%) and 1200/150 (7.13%), ultrasonic vibrations do not seem to have a positive impact on welding load reduction. Primarily at and close to optimum welding parameters (800/100 and 800/150), the amount of heat input imparted into the weldment matches well that required to have enough material softening. At a lesser weld pitch ratio (600/100), the heat addition into the weld region, even after the addition of acoustic energy, is insufficient, leading to inadequate material softening and lesser alteration in welding load. However, at a higher rotation speed, the material has already been softened to a higher amount owing to excess heat input at higher tool rotation. Therefore, ultrasonic vibrations in context to the welding load

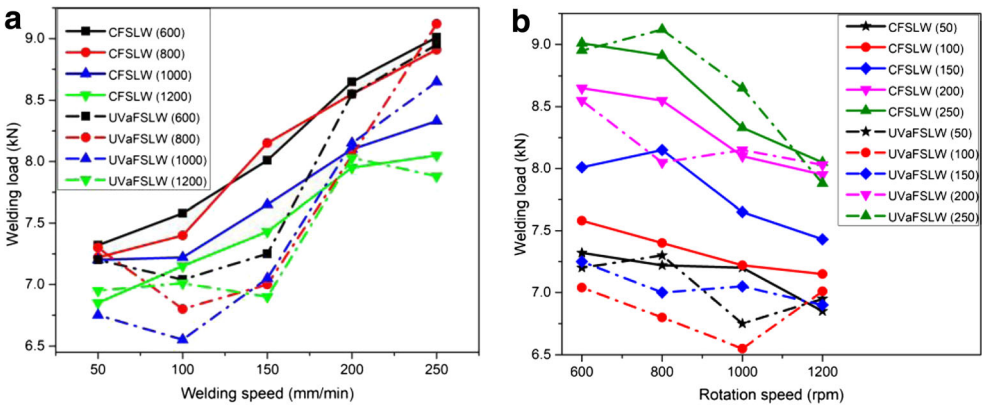

Fig. 3 Welding load variation for CFSLW and UVaFSLW at **a** constant rotation speed (600–1200) and different welding speeds (50–250) and **b** constant welding speed (50–250) and different rotation speeds (600–1200)

are proven beneficial at and close to optimum welding parameters and less responsive on other parametric combinations.

3.1.2 Torque analysis

Figure 4 portrays a variation in tool torque (peak-to-peak comparison for a given parameter) with and without ultrasonic under 800/100 and 800/150. It can be observed that with ultrasonic assistance, maximum diminution in tool torque is obtained during pin plunging at 800/100 and 800/150 equal to 22 and 9.89%, respectively. It is because ultrasonic vibrations imply localized acoustic softening of the material just below the tool pin. This alleviates the tool pin to rotate into the softened region with lesser resistance. No substantial drop in tool torque is perceived during shoulder plunging and tool travel in the case of UVaFSLW of 800/100 and 800/150 (Fig. 4a, b). As material has been softened enough during pin plunging, this leaves no space for ultrasonic vibration to further soften the material in case of shoulder plunging and during travel.

Figure 5 depicts the tool torque variation (peak-to-peak comparison for a given parameter) at different welding speeds from 50 to 250 mm/min (rotation speed constant 800 rpm, Fig. 5a) and at different rotation speeds from 600 to 1200 rpm (welding speed constant 100 mm/min, Fig. 5b). It can be observed that ultrasonic vibration is proven fruitful on specific welding parameters only in terms of maximum and minimum values. For example, a noteworthy torque reduction is obtained at 800/150, 800/200, and 1000/100, while on some parameters (800/250, 1200/100), ultrasonic vibrations seem to have negative outcomes.

3.1.3 Input power

Figure 6 shows variation in the input power (peak-to-peak comparison for a given parameter) for CFSLW and UVaFSLW at 800/100 and 800/150 welding parameters. It is apparent that ultrasonic vibrations facilitate an appreciable reduction in input power equal to 22 and 9.89% during pin plunging for 800/100 and 800/150, respectively. It is because ultrasonic vibrations imply localized acoustic softening of the material just below the tool pin. This alleviates the tool pin to rotate into the softened region with lesser resistance and lesser power requirement. No substantial reduction in input power is perceived during shoulder plunging and tool travel in the case of UVaFSLW of 800/100 and 800/150 (Fig. 6a, b). As material has been softened enough during pin plunging, this leaves no space for ultrasonic vibration to further soften the material in case of shoulder plunging and tool traveling. Figure 7 depicts the tool torque variation (peak-to-peak comparison for a given parameter) at different welding speeds from 50 to 250 mm/min (rotation speed constant, 800 rpm) and at a different rotation speed from 600 to 1200 rpm (welding speed constant, 100 mm/min). It can be observed that ultrasonic vibrations are proven fruitful on specific welding parameters only in terms of maximum and minimum values. For example, a noteworthy reduction in input power is obtained at 800/150, 800/200, and 1000/100. While on some parameters (800/250, 1200/100), ultrasonic vibrations are shown to have negative outcomes.

From the above discussion, it can be summarized that acoustic energy is proven beneficial while working at optimum parameters in context to reduction in welding load, torque, and power. Beyond that, ultrasonic assistance apparently poses minor or no effects. Acoustic softening of the material is the major cause in diminution of welding load, torque, and power.

3.2 Shear testing

Figure 8 depicts a comparative analysis of Al/Mg weldment shear failure load for CFSLW and UVaFSLW. Outcomes of different welding speeds ranging from 50 to 250 mm/min (keeping rotation speed constant, 800 rpm) and different rotation speeds varying from 600 to 1200 rpm (keeping welding speed constant, 100 mm/min), respectively, are presented. It is

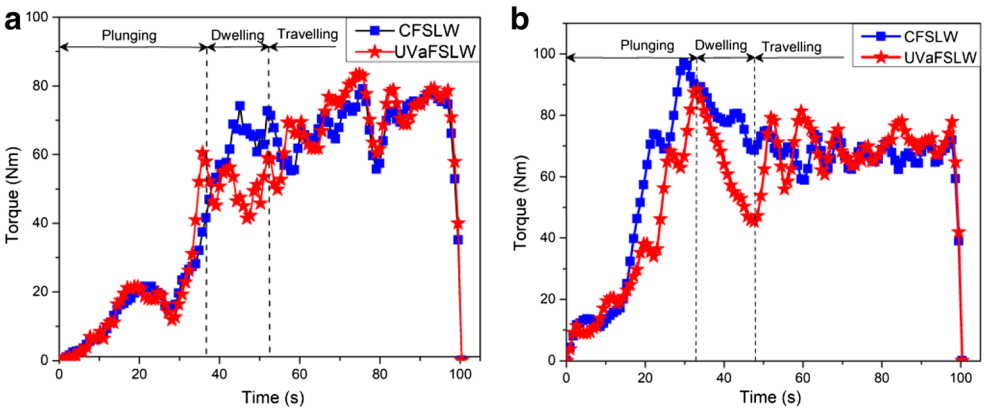

Fig. 4 Variation in tool torque for CFSLW and UVaFSLW under **a** 800 rpm and 100 mm/min and **b** 800 rpm and 150 mm/min

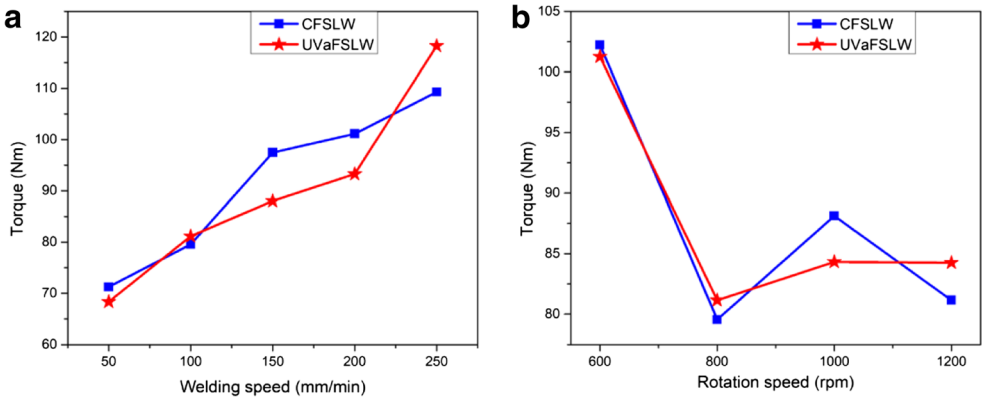

Fig. 5 Variation of tool torque at **a** constant rotation speed of 800 rpm and variable welding speed of 50–250 mm/min and **b** constant welding speed of 100 mm/min and variable rotation speed of 600–1200 rpm

observed that ultrasonic vibrations have a notable effect on the weldment shear failure load while working at optimum welding parameters. During UVaFSLW, maximum improvement in Al/Mg weldment shear strength takes place at optimum parameter (800/100), equal to 37.88%, while the same comes out 12.57, 25.40, 14.10, and 0.72% at 800/50, 800/150, 800/200, and 800/250, respectively (Fig. 8a). It is worth noting that optimum parameters reported in the current study are severely dependent on the selection of tool material, its geometry which in turn is a function of heat imparted, and strain rate at the weldment.

It can be notified that with ultrasonic assistance at 800/50 and 800/100, the weldment shear failure load is apparent to enhanced; nevertheless, the same is reported to be decreased while moving beyond 800/100, i.e., 800/150, 800/200 to 800/250. This can be explained by the fact that heat addition into the weldment is decreased with an increase in welding speed (from 50 to 100 mm/min) due to lesser time to input heat into the weldment. At lower welding speed, (800/50), the magnitude of heat input is higher than that of the optimum value to incur sound welds. Excess heat input leads to the occurrence of weldment defects. It also facilitates thickening of IMCs; hence, shear failure load of Al/Mg alloy weldment degrades gravely. At higher welding speed (800/100), the heat input into the weldment matches well the optimum value required to have a sound and defect-free weld. Optimum heat addition leads to a reduced grain size, resulting in higher weldment strength with lower strain [49–51]. At higher welding speed beyond 100 mm/min (150–250 mm/min, the constant rotation speed of 800 rpm), heat input into the weldment is reduced [52]. It leads to inadequate intermixing of Al and Mg alloys across the interface; consequently, weldment strength degrades severely.

Figure 8b portrays a comparison of Al/Mg alloy weldment shear failure load with and without ultrasonic assistance at different rotation speeds varying from 600 to 1200 rpm (keeping welding speed constant, 100 mm/min), respectively. With ultrasonic assistance, the maximum increment in shear failure load is accounted to occur at 800/100, equal to 37.88%, while on other parameters such as 600/100, 1000/100, and 1200/100, it comes out 4.92, 11.98, and − 16.82%. It can be noted that ultrasonic vibrations seem to have a negative impact on Al/Mg weldment shear strength at higher rotation speed and led to a diminution in shear failure load.

As discussed, weldment shear strength represents decreasing portray beyond 800 rpm (which is the optimum rotation speed) up to 1200 rpm (both in CFSLW and UVaFSLW). It can be inferred from the fact that higher rotation speed (beyond 800 rpm) inputs excess heat into the weldment. It causes an abrupt increase in grain size which consequently deteriorates the weld strength. Besides, it can also be theorized that higher heat input at higher rotation speed facilitates a highly conductive scenario for the formation of IMCs, which substantially weakens joint strength [53].

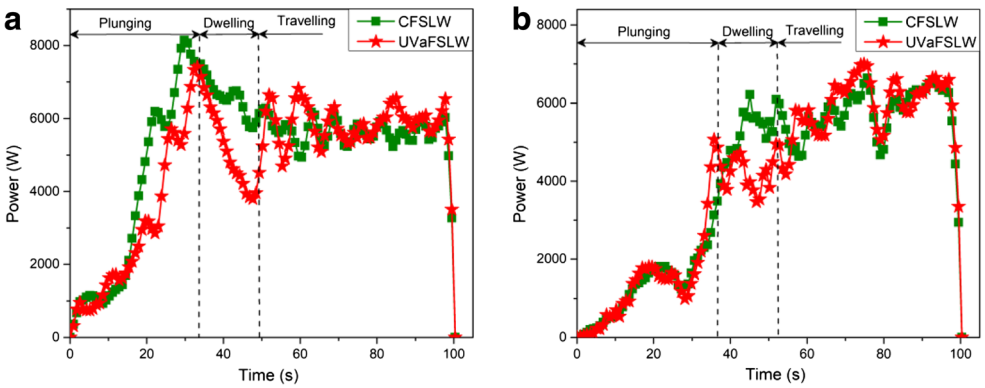

Fig. 6 Power input during CFSLW and UVaFSLW at **a** 800 rpm and 150 mm/min and **b** 800 rpm and 100 mm/min

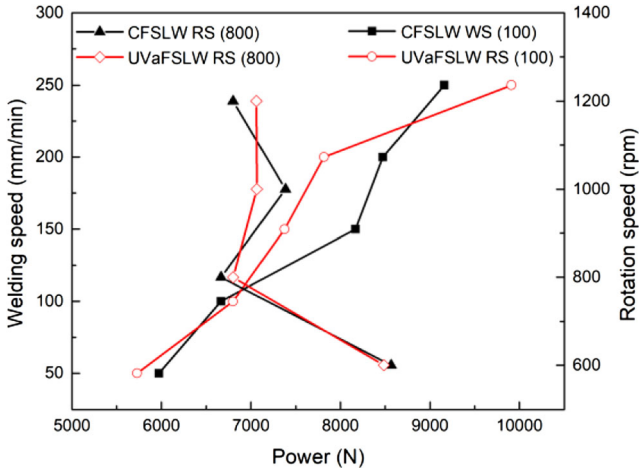

Fig. 7 Variation of input power at constant rotation speed (RS) of 800 rpm and variable welding speed of 50–250 mm/min and constant welding speed (WS) of 100 mm/min and variable rotation speed of 600–1200 rpm

In this section, Al/Mg weldment elongation is determined to visualize the effects of ultrasonic vibrations over CFSLW.

Weldment elongation is calculated and compared for different welding speeds from 50 to 250 mm/min (at a constant rotation speed of 800 rpm) and different rotation speeds ranging from 600 to 1200 rpm (at a constant welding speed of 100 mm/min) as shown in Fig. 9a, b. It is observed that ultrasonic vibrations have a significant impact on improving weldment elongation, resembling maximum improvements of 39.24% at 800/150. On other parameters such as 800/50, 800/100, 800/200, and 800/250 and 600/100, 1000/100, and 1200/100, it is reported to be equal to 11.66, 25.77, 21.36, and 10.62% and 10.25, 15.24, and 6.33%, respectively. It can be noted that at higher welding speed 800/250 and higher rotation speed 1000/100, ultrasonic vibration does not seem to have a positive impact to meliorate weldment elongation. Weldment elongation follows a decreasing trend either due to lesser (at higher welding speed, beyond 250 mm/min) or excess (at higher rotation speed, beyond 1000 rpm) heat input. It should be noted that in most of the cases, ultrasonic vibrations are incurred beneficial for improving Al/Mg weldment elongation.

3.3 Microhardness

Figure 10 shows the microhardness variation profile for Al/Mg CFSLW and UVaFSLW joints made at 800/100. Measurements are done at different locations (1 mm above (red line A) and 1 mm below (red line B) the Al/Mg weldment lap interface). It is observed that ultrasonic vibrations have the marginal effect to increase weldment microhardness. It could be understood due to ultrasonic-assisted localized softening, severe plastic deformation, and higher grain refinement of the

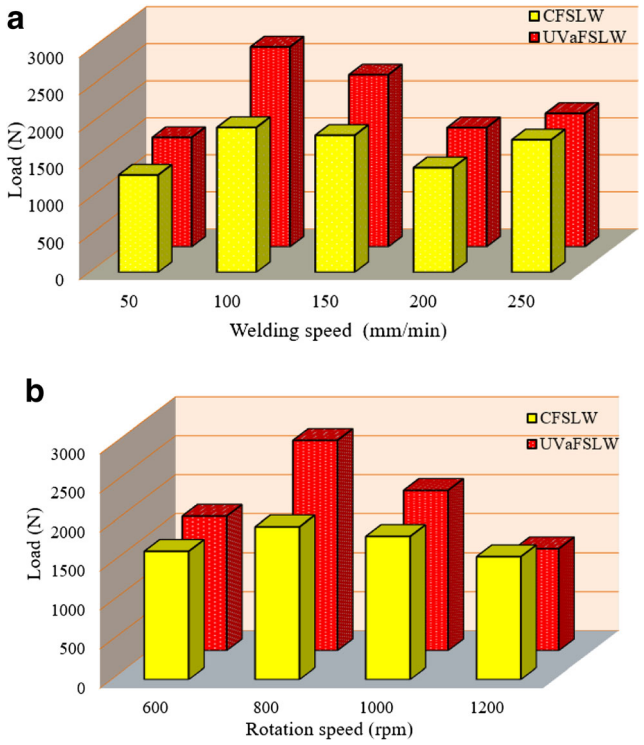

Fig. 8 Shear failure load of CFSLW and UVaFSLW Al/Mg weldments at **a** variable welding speed from 50 to 250 mm/min and constant rotation speed 800 rpm and **b** variable rotation speed from 600 to 1200 rpm and constant welding

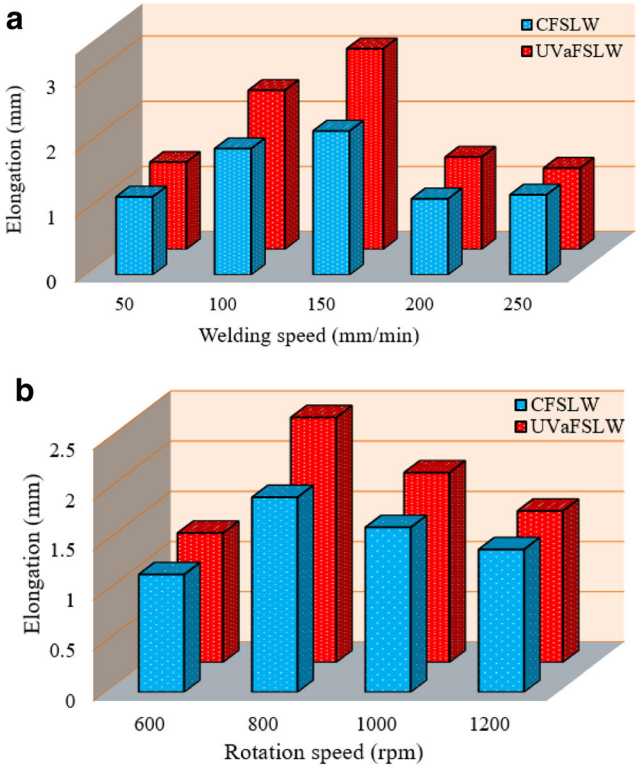

Fig. 9 Prediction of CFSLW and UVaFSLW Al/Mg weldment elongation at **a** variable welding speed from 50 to 250 mm/min and constant rotation speed 800 rpm and **b** variable rotation speed from 600 to 1200 rpm and constant welding speed 100 mm/min

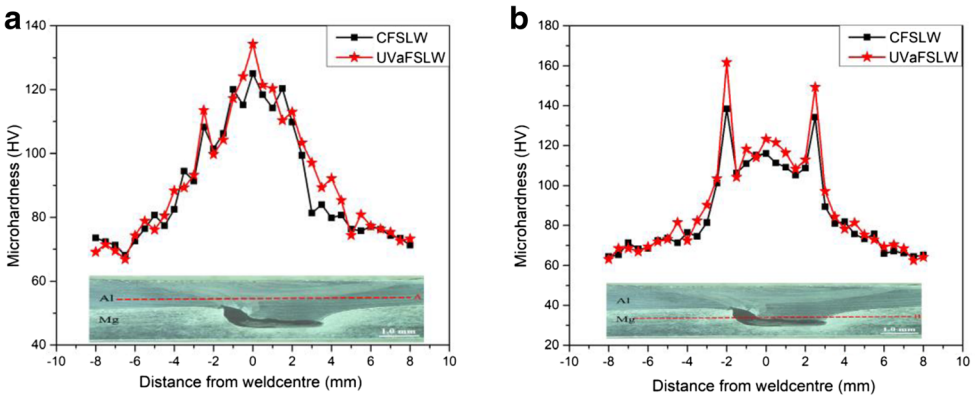

Fig. 10 Microhardness profile of Al/Mg weldment for CFSLW and UVaFSLW at 800/100 mm **a** above 1 mm from Al/Mg interface (along line A) and **b** below 1 mm from Al/Mg interface (along line B)

weldment. At the weld center, along line A (Fig. 10a), the hardness of the UVaFSLW joint is higher than that of CFSLW. No sharp peaks are observed in microhardness values, as line A does not encounter any IMC compounds in its path. While moving towards TMAZ, away from WNZ, a marginal betterment in hardness is evident in case of ultrasonic assistance. Towards the base metal, beyond TMAZ, the hardness profile shows similar (for UVaFSLW and CFSLW) variation with minor ups and downs at different points.

It can be noted that the microhardness at the weld center is quite improved for UVaFSLW compared to CFSLW. Besides, the microhardness profile portrays sharp peaks close to TMAZ, which can be attributed to the presence of the intermetallic compound. It has been established that dissimilar CFSLWs of Al and Mg alloys portray irregularly shaped regions in the WNZ and represent completely different microstructure and hardness compared to base metals. Irregularly shaped regions contain a large volume of IMCs $Al_{12}Mg_{17}$. IMCs are supposed to be formed due to constitutional liquidation and are responsible for higher hardness in WNZ [21]. The similar sharp rise in microhardness has also been reported by Mohammadi et al. [18] during the CFSLW of Al/Mg. Towards the base metal, away from TMAZ, the microhardness profile seems to have quite similar values for both CFSLW and UVaFSLW.

3.4 Macrostructure and weld morphology

Figure 11 shows the macrostructure profile of CFSLW and UVaFSLW Al/Mg weldments made at 800/100, 1000/100, and 600/100, respectively. It is clearly observed that a significant degree of material intermixing occurred between Al and Mg alloys as a result of the penetration of the tool pin into the lower sheet. The WNZ of the Al/Mg joint seems to portray a bowl-like morphology due to a tapered-threaded pin and concave shoulder profile. It can be observed that the WNZ bowl morphology is more intense and well defined (in terms of size and shape) in case of ultrasonic assistance. At the retreating side (RS), the bowl shape of the WNZ is truncated (point C) due to the absence of the required weldment turbulence, and the same seems to be nullified in case of ultrasonic assistance (point D). It could be because of insufficient turbulence into the WNZ during tool advancement. While in the presence of ultrasonic assistance, an additional weldment pulsation is

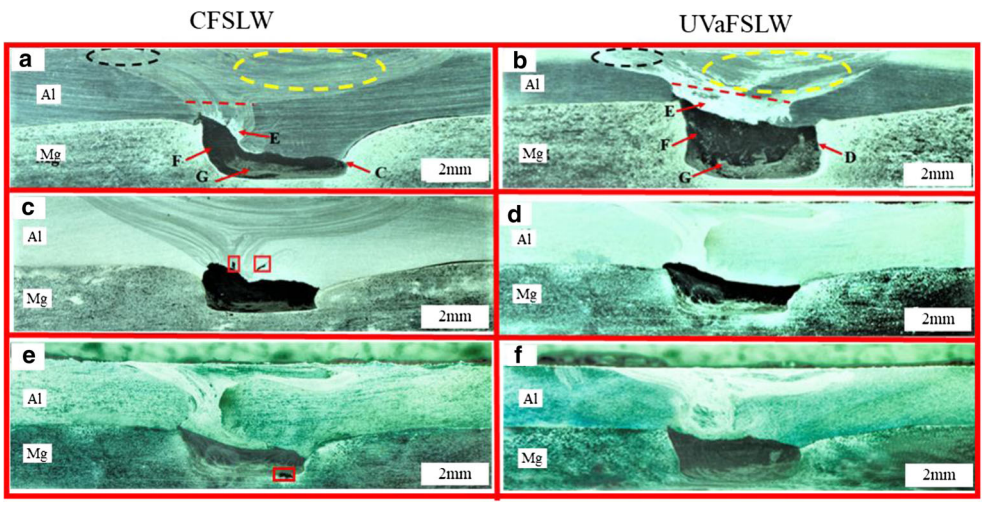

Fig. 11 Macrostructure evaluation of Al-Mg weldments at **a**, **b** 800/100, **c**, **d** 1000/100, and **e**, **f** 600/100. C, broken bowl morphology; D, well-defined bowl morphology; E, white structures; F, Al-rich black structures; G, Mg-rich brown structures

originated [54], which leads to enhanced acoustic softening [55] as well as metal releveling. The bowl-shape morphology also contains an intermixed region of black (Al-rich) and brown (Mg-rich) (represented by F and G) colored metal structure at its bottom. It could be the replica of intense material mixing of dissimilar metals. The volume percentage of the black and brown-colored region is much higher in case of ultrasonic assistance (F and G) compared to CFSLW (Fig. 11a, b). It evidences that during ultrasonic assistance, the comparatively large volume of both the metals is taken away from their faying surfaces and intermixed into the WNZ. The dissimilar intermixed material evidently settles down at a lower portion of the bowl-shaped WNZ. Material flow beneath the tip of the rotating pin promotes a "swirl zone" [56] which represents a bottom portion of the bowl structure. As the WNZ is the region where intense mixing of Al/Mg alloys occurs, it leads to the formation of lamellar structures into it. A relatively white-colored structure appeared in the WNZ [57] (region E) which represents a high degree of intermixing of Al and Mg alloys. The volume percentage of white-colored structures appeared to be significantly larger in the case of UVaFSLW compared to CFSLW. It further ensures that ultrasonic assistance facilitates intense material mixing in the WNZ even in the case of dissimilar metals. A small portion of the Mg metal (both at the advancing side (AS) and RS) seems to bend upwards to penetrate into the Al metal. This feature is called hook, which has also been reported in past literature in context to friction stir lap or spot welding [58]. The effect of ultrasonic assistance can also be realized by comparing the material flow path into the WNZ adjacent to the pin (PR) (shown in red dashed lines). From Fig. 11a, b, it can be observed that PR appears to be wider in the case of UVaFSLW compared to CFSLW. A close observation reveals that PR in the case of ultrasonic assistance (PRuv) comes out to be 2.50 mm compared to 4.13 mm in the case of CFSLW (PRc). It depicts a rise of 65.20% material movement adjacent to the pin surface with ultrasonic assistance. AS PRuv is larger than PRc for a given parameter, indicating that the volume of deformed material across the pin surface increases when ultrasonic vibrations are integrated into the CFSLW. Another vital observation derived from Fig. 11a, b is the shape of the WNZ bowl. It can be observed that the bowl trajectory area during CFSLW is quite less than that shown in the case of UVaFSLW. It infers that ultrasonic vibration enhances the material mixing as well as enhances the material flow which widens the trajectory area of the bowl. It has been evidently proven that material viscosity and thereby material flow stresses are reduced when ultrasonic vibration is integrated into the CFSW process [36]. These constituents enhance material deformation, and in turn, material flow is quite improved [36]. Another outcome can be derived by comparing WNZ regions at the AS (dashed black region) and RS (dashed yellow region) sides for CFSLW and UVaFSLW. It can be observed that in the absence of ultrasonic, the WNZ (region represented by black and yellow dashed lines at AS and RS) does not seem to have adequate material flow and white structures, while in the addition of ultrasonic assistance, an intense material flow is evident with quite a higher percentage of white structures. From macrostructure analysis, a rise in shear strength of the welded specimen in the presence of acoustic energy can be understood by the fact that the WNZ bowl contains a larger volume of Al and Mg intermixed compounds compared to CFSLW. It poses significantly higher resistance to shear during shear testing of the welded samples. Consequently, the shear strength of UVaFSLW joints is notably higher than that of CFSLW joints as depicted in Section 3.2.

Figure 11c–f depicts the macrostructures of transverse sections of the untested joints produced at rotation speeds of 1000/100 and 600/100 for CFSLW and UVaFLSW. Microvoids are distinctly ascertained in the CFSLW joint (Fig. 11c, e; red color rectangles). It is because a higher tool rotation and lower tool travel speed lead to the input of an excessive amount of heat into the WNZ. It facilitates cavity formation, as excessive heat generated would make it easier for the deformed materials to be excreted on the surface as flash [59, 60]. The lower failure load at 1000/100 CFSLW could be ascertained to the formation of cavities across dissimilar metal interfaces. A comparatively high rotation to welding speed ratio results in unreasonable heat addition into the SZ and leads to the formation of cavities, as the deformed metals have undergone on the metal surface in the form of flash [24]. As the weld formed at 1000/100 failed through shear overload (as depicted in Section 3.2), the hook feature having an inward slope poses the least resistance for shear deformation. The weld produced at 600/100 shows large cavities both at AS and RS and results into abnormal material mixing due to poor heat input (Fig. 11e). The weld made at 800/100 shows a structurally sound joint without any presence of a channel or cavity defects; additionally, the cold lap and outward hook geometry favors enhancement in weldment strength (Fig. 11a). Microvoids disappear in lap joints treated with ultrasonic assistance (UVaFSLW) Fig. 11d, f. It is because ultrasonic vibration induces a significant amount of additional turbulence into the WNZ [54] such that plasticized metal adjusts itself to fill up the cavities or gaps formed during the welding cycle.

Weld appearance for Al-Mg weldments for CFSLW and UVaFSLW at 800/100, 1000/100, and 600/100, respectively, is shown in Fig. 12. It is apparent that at 800/100, the weldment top surface looks smooth and has a good appearance, while on other parameters the surface quality is bad with a poor surface finish. For 1000/100 and 600/100, the weld surface is uneven, with the presence of a zig-zag line, reflecting inadequate material intermixing as well as heavy flush pulled out while welding. With ultrasonic assistance, the surface appearance of the weldment is quite improved as well as the

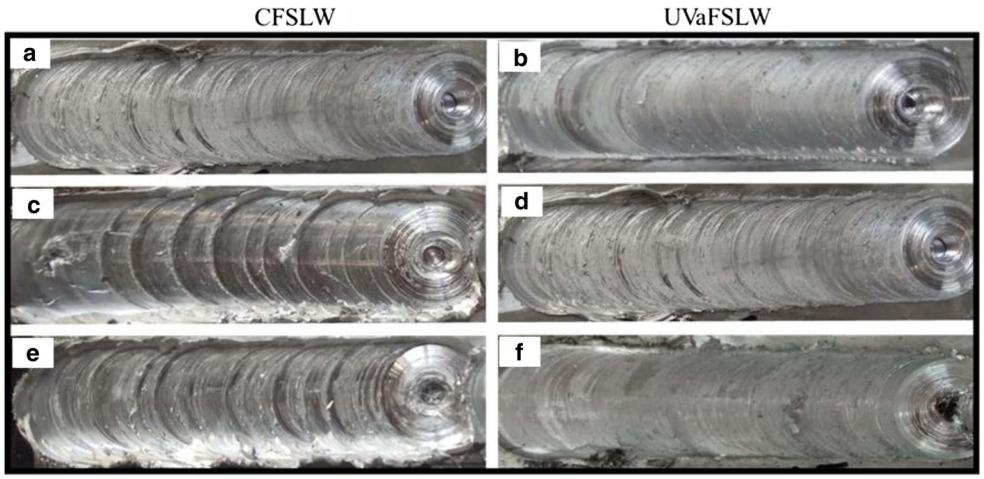

Fig. 12 Al-Mg weldments at **a**, **b** 800/100, **c**, **d** 1000/100, and **e**, **f** 600/100

surface defects apparently will be eliminated. Material mixing in the case of ultrasonic assistance is quite homogeneous, and both the alloys seemed to be penetrating each other well.

3.5 Fractography

In order to determine and compare the fracture properties of CFSLW and UVaFSLW Al-Mg weldment, fracture analysis of tested samples is performed at 800/100. It is observed that the CFSLWed joint failed via shear and tensile fracture mode. This failure mode is characterized by dual-path crack propagation, via lap interface and through the hook. However, in the present scenario, a prominent fracture seems to be observed across the dissimilar metal interface. After application of acoustic energy into the weldment, the failure is observed to occur via tensile fracture, away from the SZ of both the metals. Such failure is characterized by crack initiation across the hook followed by its propagation along TMAZ. In order to enable a deep understanding of the mechanism involved during fracture of Al-Mg alloys with and without ultrasonic vibrations, SEM analysis of fractured surfaces is presented as shown in Fig. 13a.

The occurrence of a shear failure mechanism due to poor intermixing as well as diffusion of atoms of both lapped metals is characterized [61], emphasizing the weak bonding of both Al and Mg alloys together. SEM imaging of the fracture surface reflects the presence of fluffy voids as well as tearing ridges depicting load sustainability during microvoid coalescence leads to localized brittle fracture [62]. On a wide portray is the presence of a mixed mode of ductile-brittle fracture. SEM imaging of the fracture surface of UVaFSLWed joints is portrayed in Fig. 13b. An obvious presence of a ductile fracture pattern with coalescence of wide-sized deep dimples is evident. A moderate population of dimples oriented in the shear zone is observed and could be the replicable path of crack propagation. Thereby, on a broad scenario, the failure mode of the sample can be considered to be distinctly ductile in nature.

4 Conclusions

(1) With ultrasonic assistance, a considerable drop in welding load and tool torque is obtained at optimum parameters, 800/100 and 800/150 equal to 29.32, 22.12, and 30.01, 19.75% during pin and shoulder plunging, respectively.

(2) Maximum improvement in shear strength of Al/Mg weldment with ultrasonic assistance apparently occurs at

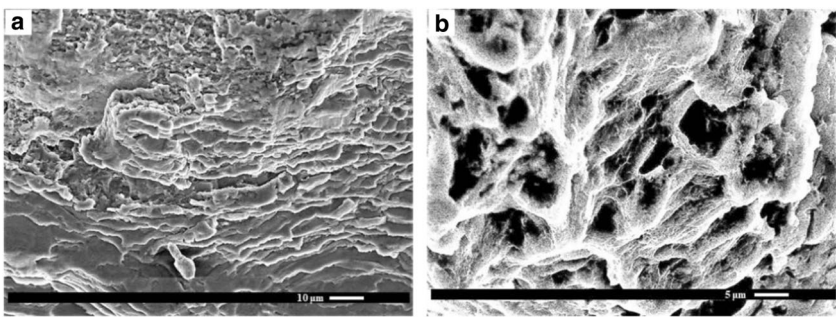

Fig. 13 SEM image of the fracture surface at 800/100 **a** CFSLW and **b** UVaFSLW

800/100, equal to 37.88%. However, ultrasonic vibrations seem to pose negative influence in weldment shear strength at higher rotation speeds.

(3) Ultrasonic vibration seems to have marginal effects on weldment microhardness. In the regions, where IMCs are observed to be present, a sudden rise in microhardness is reported.

(4) Intense material mixing and enhanced material flow are depicted in the vicinity of the WNZ. Besides, truncation in the WNZ bowl trajectory is found to be replaced with well-defined and more prominent material stirring during ultrasonic assistance. The constitution of dispersed and mixed IMCs in SZ, as well as disruption in the presence of ultrasonic vibrations, favors weldment property enhancement.

Acknowledgements The authors acknowledge the financial support from the Key R&D Program of Shandong Province in China (Grant No. 2018GGX103001).

References

1. Kumar S, Wu CS (2017) Review: Mg and its alloy—scope, future perspectives and recent advancements in welding and processing. J Harbin Inst Technol (New Ed) 24:1–37
2. Afghani SSS, Jafarian M, Paidar M, Jafarian M (2016) Diffusion bonding of Al 7075 and Mg AZ31 alloys: process parameters, microstructural analysis and mechanical properties. Trans Nonferrous Met Soc China 26:1843–1851
3. Atabay SE, Esen Z, Dericioglu AF (2017) Effect of Sn alloying on the diffusion bonding behavior of Al-Mg-Si alloys. Metall Mater Trans A 48:3181–3187
4. Gao Q, Meco S, Wang K, Guo S (2017) Light-weight Mg/Al dissimilar structures welded by CW laser for weight saving applications. In: Advanced computational methods in life system modeling and simulation. Springer, Singapore, pp 349–357
5. Islam MR, Ishak M, Shah LH, Idris SRA, Meriç C (2017) Dissimilar welding of A7075-T651 and AZ31B alloys by gas metal arc plug welding method. Int J Adv Manuf Technol 88:2773–2783
6. Singh K, Singh G, Singh H (2018) Review on friction stir welding of magnesium alloys. J Magnes Alloy
7. Zhen S, Wu CS, Kumar S (2018) Determination of heat generation by correlating the interfacial friction stress with temperature in friction stir welding. J Manuf Process 31:801–811
8. Anil Kumar KS, Murigendrappa SM, Kumar H (2017) A bottom-up optimization approach for friction stir welding parameters of dissimilar AA2024-T351 and AA7075-T651 alloys. J Mater Eng Perform 26:3347–3367
9. Liu X, Sun Y, Morisada Y, Fujii H (2018) Dynamics of rotational flow in friction stir welding of aluminium alloys. J Mater Process Technol 252:643–651
10. Regev M, Rashkovsky T, Cabibbo M, Spigarelli S (2018) Microstructure stability during creep of friction stir welded AA2024-T3 alloy. J Mater Eng Perform:1–10
11. Shanavas S, Edwin Raja Dhas J, Murugan N (2018) Weldability of marine grade AA 5052 aluminum alloy by underwater friction stir welding. Int J Adv Manuf Technol 95:4535–4546
12. Imam M, Racherla V, Biswas K, Fujii H, Chintapenta V, Sun Y, Morisada Y (2017) Microstructure-property relation and evolution in friction stir welding of naturally aged 6063 aluminium alloy. Int J Adv Manuf Technol 91:1753–1769
13. Liu F, Fu L, Chen H (2018) High speed friction stir welding of ultra-thin AA6061-T6 sheets using different backing plates. J Manuf Process 33:219–227
14. Patel VV, Badheka VJ, Patel U, Patel S, Patel S, Zala S, Badheka K (2017) Experimental investigation on hybrid friction stir processing using compressed air in aluminum 7075 alloy. Mater Today Proc 4: 10025–10029
15. Lv X, Wu CS, Yang CL, Padhy GK (2018) Weld microstructure and mechanical properties in ultrasonic enhanced friction stir welding of Al alloy to Mg alloy. J Mater Process Technol 254: 145–157
16. Firouzdor V, Kou S (2009) Al-to-Mg friction stir welding: effect of positions of Al and Mg with respect to the welding tool. Weld J 88: 213–224
17. Chowdhury SH, Chen DL, Bhole SD, Cao X, Wanjara P (2013) Lap shear strength and fatigue behavior of friction stir spot welded dissimilar magnesium-to-aluminum joints with adhesive. Mater Sci Eng A 562:53–60
18. Mohammadi J, Behnamian Y, Mostafaei A, Izadi H, Saeid T, Kokabi AH, Gerlich AP (2015) Friction stir welding joint of dissimilar materials between AZ31B magnesium and 6061 aluminum alloys: microstructure studies and mechanical characterizations. Mater Charact 101:189–207
19. Dorbane A, Mansoor B, Ayoub G, Shunmugasamy VC, Imad A (2016) Mechanical, microstructural and fracture properties of dissimilar welds produced by friction stir welding of AZ31B and Al6061. Mater Sci Eng A 651:720–733
20. Verma J, Taiwade RV, Sapate SG, Patil AP, Dhoble AS (2017) Evaluation of microstructure, mechanical properties and corrosion resistance of friction stir-welded aluminum and magnesium dissimilar alloys. J Mater Eng Perform 26:4738–4747
21. Sato YS, Park SHC, Michiuchi M, Kokawa H (2004) Constitutional liquation during dissimilar friction stir welding of Al and Mg alloys. Scr Mater 50:1233–1236
22. Chen YC, Nakata K (2008) Friction stir lap joining aluminum and magnesium alloys. Scr Mater 58:433–436
23. Lv XQ, Wu CS, Padhy GK (2017) Diminishing intermetallic compound layer in ultrasonic vibration enhanced friction stir welding of aluminum alloy to magnesium alloy. Mater Lett 203:81–84
24. Yamamoto N, Liao J, Watanabe S, Nakata K (2009) Effect of intermetallic compound layer on tensile strength of dissimilar friction-stir weld of a high strength Mg alloy and Al alloy. Mater Trans 50: 2833–2838
25. Mohammadi J, Behnamian Y, Mostafaei A, Gerlich AP (2015) Tool geometry, rotation and travel speeds effects on the properties of dissimilar magnesium/aluminum friction stir welded lap joints. Mater Des 75:95–112
26. Rao HM, Yuan W, Badarinarayan H (2015) Effect of process parameters on mechanical properties of friction stir spot welded magnesium to aluminum alloys. Mater Des 66:235–245
27. Tan S, Zheng F, Chen J, Han J, Wu Y, Peng L (2017) Effects of process parameters on microstructure and mechanical properties of friction stir lap linear welded 6061 aluminum alloy to NZ30K magnesium alloy. J Magnes Alloy 5:56–63
28. Firouzdor V, Kou S (2010) Formation of liquid and intermetallics in Al-to-Mg friction stir welding. Metall Mater Trans A 41:3238–3251
29. Liu Z, Ji S, Meng X (2018) Improving joint formation and tensile properties of dissimilar friction stir welding of aluminum and magnesium alloys by solving the pin adhesion problem. J Mater Eng Perform 27:1404–1413

30. Shah LH, Gerlich A, Zhou Y (2017) Design guideline for intermetallic compound mitigation in Al-Mg dissimilar welding through addition of interlayer. Int J Adv Manuf Technol 1–12
31. Macwan A, Kumar A, Chen DL (2017) Ultrasonic spot welded 6111-T4 aluminum alloy to galvanized high-strength low-alloy steel: microstructure and mechanical properties. Mater Des 113: 284–296
32. Peng H, Jiang XQ, Bai XF, Li D, Chen D (2018) Microstructure and mechanical properties of ultrasonic spot welded Mg/Al alloy dissimilar joints. Metals (Basel) 8:229
33. Kumar S, Wu CS, Padhy GK (2017) Ultrasonic vibrations in friction stir welding: state of the art. In: 7th International Conference on Welding Science and Engineering (WSE 2017) in conjunction with 3rd International Symposium on Computer-Aided Welding Engineering (CAWE 2017). Shandong University, Jinan, China, pp 272–276
34. Kumar S, Wu CS, Padhy GK, Ding W (2017) Application of ultrasonic vibrations in welding and metal processing: a status review. J Manuf Process 26:295–322
35. Liu XC, Wu CS (2015) Material flow in ultrasonic vibration enhanced friction stir welding. J Mater Process Technol 225:32–44
36. Shi L, Wu CS, Liu XC (2015) Modeling the effects of ultrasonic vibration on friction stir welding. J Mater Process Technol 222:91–102
37. Kumar S (2016) Ultrasonic assisted friction stir processing of 6063 aluminum alloy. Arch Civ Mech Eng 16:473–484
38. Liu XC, Wu CS (2016) Elimination of tunnel defect in ultrasonic vibration enhanced friction stir welding. Mater Des 90:350–358
39. Liu XC, Wu CS (2014) Effect of ultrasonic vibration on microstructure and mechanical properties of friction stir welded joint of 6061-T4 aluminum alloy. Trans China Weld 35:49–53
40. Meng X, Xu Z, Huang Y, et al (2017) Interface characteristic and tensile property of friction stir lap welding of dissimilar aircraft 2060-T8 and 2099-T83 Al–Li alloys. Int J Adv Manuf Technol 1–9
41. Ji S, Meng X, Liu Z, Huang R, Li Z (2017) Dissimilar friction stir welding of 6061 aluminum alloy and AZ31 magnesium alloy assisted with ultrasonic. Mater Lett 201:173–176
42. Benfer S, Straß B, Wagner G, Fürbeth W (2016) Manufacturing and corrosion properties of ultrasound supported friction stir welded Al/Mg-hybrid joints. Surf Interface Anal 48:843–852
43. Kumar S, Wu CS (2018) A novel technique to join Al and Mg alloys: ultrasonic vibration assisted linear friction stir welding Mater Today Proc 05
44. Strass B, Wagner G, Conrad C et al (2014) Realization of Al/Mg-hybrid-joints by ultrasound supported friction stir welding—mechanical properties, microstructure and corrosion behavior. Adv Mater Res 966–967:521–535
45. Shi L, Wu CS, Liu XC (2015) Modelling the effects of ultrasonic vibrations in friction stir welding. J Mater Process Technol 222:91–102
46. Park K, Kim B, Ni J (2008) Numerical simulation of plunge force during the plunge phase of friction stir welding and ultrasonic assisted FSW. ASME 2008 International Mechanical Engineering Congress and Exposition
47. Kumar S, Ding W, Zhen S, Wu CS (2018) Analysis of the dynamic performance of a complex ultrasonic horn for application in friction stir welding. Int J Adv Manuf Technol 97:1269–1284
48. Zhong YB, Wu CS, Padhy GK (2017) Effect of ultrasonic vibration on welding load, temperature and material flow in friction stir welding. J Mater Process Technol 239:279–283
49. Ammouri AH, Kridli G, Ayoub G, Hamade RF (2015) Relating grain size to the Zener-Hollomon parameter for twin-roll-cast AZ31B alloy refined by friction stir processing. J Mater Process Technol 222:301–306
50. Commin L, Dumont M, Masse JE, Barrallier L (2009) Friction stir welding of AZ31 magnesium alloy rolled sheets: influence of processing parameters. Acta Mater 57:326–334
51. Albakri AN, Mansoor B, Nassar H, Khraisheh MK (2013) Thermo-mechanical and metallurgical aspects in friction stir processing of AZ31 Mg alloy—a numerical and experimental investigation. J Mater Process Technol 213:279–290
52. Saju TP, Ganesh Narayanan R (2018) Friction stir forming of dissimilar grade aluminum alloys: influence of tool rotational speed on the joint evolution, mechanical performance, and failure modes. Int J Adv Manuf Technol 95:1377–1397
53. Firouzdor V, Kou S (2010) Al-to-Mg friction stir welding: effect of material position, travel speed, and rotation speed. Metall Mater Trans A 41:2914–2935
54. Ahmadnia M, Seidanloo A, Teimouri R, Rostamiyan Y, Titrashi KG (2015) Determining influence of ultrasonic-assisted friction stir welding parameters on mechanical and tribological properties of AA6061 joints. Int J Adv Manuf Technol 78:2009–2024
55. Shi L, Wu CS, Padhy GK, Gao S (2016) Numerical simulation of ultrasonic field and its acoustoplastic influence on friction stir welding. Mater Des 104:102–115
56. Gerlich A, Su P, Yamamoto M, North TH (2008) Material flow and intermixing during dissimilar friction stir welding. Sci Technol Weld Join 13:254–264
57. Ji S, Li Z, Zhang L, Zhou Z, Chai P (2016) Effect of lap configuration on magnesium to aluminum friction stir lap welding assisted by external stationary shoulder. Mater Des 103:160–170
58. Rajesh S, Badheka VJ (2018) Process parameters/material location affecting hooking in friction stir lap welding: dissimilar aluminum alloys. Mater Manuf Process 33:323–332
59. Kim YG, Fujii H, Tsumura T, Komazaki T, Nakata K (2006) Three defect types in friction stir welding of aluminum die casting alloy. Mater Sci Eng A 415:250–254
60. Zhao Y, Huang L, Zhao Z, Yan K (2016) Effect of travel speed on the microstructure of Al-to-Mg FSW joints. Mater Sci Technol 32: 1025–1034
61. Zhao Y, Zhou L, Wang Q, Yan K, Zou J (2014) Defects and tensile properties of 6013 aluminum alloy T-joints by friction stir welding. Mater Des 57:146–155
62. Chen H, Fu L, Liang P, Liu F (2017) Defect features, texture and mechanical properties of friction stir welded lap joints of 2A97 Al-Li alloy thin sheets. Mater Charact 125:160–173